Oriented overgrowth of pharmacolite ($CaHAsO_4 \cdot 2H_2O$) on gypsum ($CaSO_4 \cdot 2H_2O$)

ARTICLE *in* CRYSTAL GROWTH & DESIGN · NOVEMBER 2007

Impact Factor: 4.89 · DOI: 10.1021/cg070222+

3 AUTHORS:

Juan Diego Rodriguez-Blanco
University of Copenhagen
42 PUBLICATIONS **539** CITATIONS
SEE PROFILE

Amalia Jiménez
University of Oviedo
39 PUBLICATIONS **357** CITATIONS
SEE PROFILE

Manuel Prieto
University of Oviedo
109 PUBLICATIONS **1,550** CITATIONS
SEE PROFILE

CRYSTAL GROWTH & DESIGN
2007
VOL. 7, NO. 12
2756–2763

Oriented Overgrowth of Pharmacolite ($CaHAsO_4 \cdot 2H_2O$) on Gypsum ($CaSO_4 \cdot 2H_2O$)

Juan Diego Rodríguez-Blanco, Amalia Jiménez,* and Manuel Prieto

Departamento de Geología, Universidad de Oviedo, Jesús Arias de Velasco s/n, 33005 Oviedo, Spain

Received March 7, 2007; Revised Manuscript Received August 31, 2007

ABSTRACT: At neutral pH and 25 °C, the interaction of arsenate-bearing aqueous solutions with gypsum results in surface precipitation of pharmacolite ($CaHAsO_4 \cdot 2H_2O$) crystals. The crystals grow oriented onto the gypsum surface, forming an epitaxy. Using an *A*-centered unit-cell setting for both pharmacolite (*Aa*) and gypsum (*A2/a*), the epitaxial relationship is found to be $(010)_{Gy} \parallel (0\bar{1}0)_{Ph}$ and $[101]_{Gy} \parallel [101]_{Ph}$. Pharmacolite forms thick three-dimensional crystals elongated on [101] with {010}, $\{\bar{1}11\}$, and $\{1\bar{1}\bar{1}\}$ as major forms. Both the crystal morphology and the epitaxial orientation are interpreted on the basis of the bond arrangement in the structure of both phases. The reaction can be envisaged as a sort of solvent-mediated replacement of gypsum by pharmacolite. Under these experimental conditions, the process stops at a "pseudo-equilibrium" end point in which the reactive solids become completely isolated from the aqueous solution by the epitaxial coating of pharmacolite crystals. The thermodynamic solubility product of pharmacolite was determined at this stage and found to be $pK = 4.68 \pm 0.04$. The reaction paths actually followed by the system and the "true equilibrium" end point are modeled using the geochemical code PHREEQC.

Introduction

Cocrystallization from aqueous solutions has been receiving increasing attention in a variety of research fields, particularly in environmental chemistry. When two solutes crystallize simultaneously and have similar crystal structures, the formation of solid solutions and/or epitaxial intergrowths is always a possibility, which is interesting not only from a fundamental point of view but also from an applied perspective. For instance, the uptake of dissolved metals by precipitation of metal-bearing solid solutions on mineral surfaces has been widely investigated as a potential method to remove toxic metals from polluted waters.[1–4] In these studies, a metal-containing aqueous solution is placed in contact with mineral fragments, and the subsequent surface precipitation is envisaged as a sorption process[5] in which the sorbate is an adherent, crystalline phase that consists of chemical species derived from both the aqueous solution and the dissolution of the mineral. The effectiveness of these processes depends not only on the thermodynamics of the involved system but also on the spatial arrangement and crystallographic relations between substrate and overgrowth.[6]

Recently, the formation of solid solutions of anionic substitution has been investigated to assess the environmental behavior of Cr(VI), Se(VI), and other oxyanions.[7–9] In the same way, Roman-Ross and co-workers[10,11] have recently studied the precipitation of gypsum by mixing $CaCl_2$ and Na_2SO_4 aqueous solutions in the presence of dissolved Na_2HAsO_4 and have detected the incorporation of some arsenate (substituting for sulfate) into the gypsum structure. This incorporation supposes an increase of the unit cell parameters, since AsO_4^{3-} (or $HAsO_4^{2-}$) is considerably greater than SO_4^{2-}. In conclusion, these authors suggest that As(V) could be sorbed onto gypsum by forming a limited calcium arsenate-sulfate solid solution. The existence of a certain connection between arsenate and gypsum has also been observed by Juillot and co-workers,[12] who, in studying the remobilization of arsenic from buried wastes at an industrial site, have observed an intimate association of gypsum and calcium arsenates, detecting that gypsum may contain some arsenic and calcium arsenates may contain some sulfur.

The present work is part of a broader research proposal[13] on the interaction of As(V) with gypsum at different pH ranges. At basic pHs, the prevailing aqueous species are AsO_4^{3-} and $HAsO_4^{2-}$, and this interaction results in surface precipitation of a diversity of calcium arsenates, including $Ca_5(HAsO_4)_2(AsO_4)_2 \cdot 9H_2O$ (guerinite or ferrarisite), $Ca_5(HAsO_4)_2(AsO_4)_2 \cdot 4H_2O$ (sainfeldite), double salts such as $NaCaAsO_4 \cdot 7.5H_2O$ and amorphous calcium arsenate hydrates. Because of the arsenic toxicity,[14] arsenates[15] and particularly calcium arsenates have been widely investigated,[16–18] but numerous issues remain unresolved. Whereas the pH ranges in which AsO_4^{3-}, $HAsO_4^{2-}$, or $H_2AsO_4^{-}$ are the prevailing charged species are well established, the crystal chemistry and the crystallization behavior of many calcium arsenates remain largely unknown. Moreover, with some significant exceptions,[19] the determination of thermodynamic solubility products of arsenates has received little attention, perhaps as a consequence of the complicated crystallization behavior of these compounds in aqueous environments, which involves formation of an enormous diversity of hydrates, double salts, presence of arsenate groups with different protonation degrees, etc. Here we focus on the interaction between gypsum and As(V) at intermediate pHs. It is generally admitted that at $pH < 8$ there is a tendency to form fairly soluble acidic arsenates which are not of interest as environmental remediation tools.[20] However, the nature, solubility, and crystallization behavior of the solid phases that precipitate in this pH range need to be investigated, as well as the possible formation of mixed crystals and/or intergrowths with gypsum.

Experimental Procedures

Interaction experiments were carried out at 25 ± 0.05 °C and at atmospheric pressure by reacting gypsum grains with an As(V)-bearing aqueous solution in a thermostatted and continuously stirred (100 rpm) polypropylene vessel. The parent solution was prepared by adding NaOH to a 100 mM H_3AsO_4 (Merck) aqueous (MilliQ) solution until the desired initial pH of 7.0 was reached. Then 2.000 ± 0.005 g of mineral grains with diameters ranging from 1.0 mm up to 1.5 mm were added to 100 cm^3 (weighed to 0.001 g) of solution. Finally, the vessel

* Corresponding author: Tel.: (+34) 985 109552. Fax: (+34) 985 103 103. E-mail:amalia.jimenez@geol.uniovi.es.

10.1021/cg070222+ CCC: $37.00
Published on Web 11/20/2007

was closed and sealed with a polypropylene cap to avoid contact with the atmosphere and minimize evaporation. The experiment was repeated five times (starting from a mutual parent solution) to examine the reproducibility of the process. Thus, all the reported analytical results represent the average of five analogous experimental runs.

Gypsum grains were prepared by crushing natural single crystals. The obtained fragments were sieved to the selected size range and ultrasonically cleaned in an ethanol bath. This starting material was confirmed to be gypsum by X-ray diffraction (XRD, Philips-X′Pert-PRO) and analyzed by X-ray fluorescence spectroscopy (XRF, Philips-PW2404). XRF analyses yielded less than 0.2 wt% foreign elements, with Na, Sr, and P as the major impurities. The grains were essentially cleavage fragments dominated by (010) crystal faces and were determined to have a specific N_2-BET (Micrometrics-ASAP-2010) surface area of 0.16 $m^2\ g^{-1}$. The choice of cleavage fragments with smooth surfaces within this size range was aimed to minimize the significance of adsorption in comparison with surface precipitation.

The experiments proceeded for 20 days, and the pH was continuously monitored during this time. Moreover, after the predetermined reaction periods, 1 mL aliquots of solution were taken and assayed for dissolved calcium, sodium, sulfate, and arsenic. The solution pH was measured with a combination electrode (Ross-Thermo-Orion-810200) and a digital pH-meter (CyberScan-pH-2100). Dissolved arseniate and sulfate were determined by ionic chromatography (Metrohm Advanced Compact 861 IC), whereas Ca and Na were measured by atomic absorption spectrometer (AAS, Pye-Unicam-SP-90). The results are rather reproducible, particularly in the case of arsenic. The variation in arsenic concentration from replicate experiments of the same reaction time was less than ±4% (RSD). For sulfate, calcium, and sodium this variation was found to be within ± 6%. Speciation and aqueous solution modeling was carried out using PHREEQC,[21] a geochemical modeling program based on the ion-association aqueous model with a diversity of capabilities.

During and after the experiments, representative individuals of the gypsum grains were selected with the help of a stereomicroscope (Leica MZ75) and removed from the aqueous solution to verify the incorporation of As-bearing solid phases on their surfaces. With this aim, the grain surfaces were examined through a scanning electron microscope (SEM, Jeol-JSM-6100). This SEM was also used to estimate the composition of the precipitates using an INCA Energy 200 microanalysis system (EDS) with a silicon detector (PentaFET, Oxford Instruments) fitted with an ultrathin window that allows the detection of oxygen. SEM observations were combined with glancing incidence and powder XRD (Philips-X-Pert-PRO; Seifert XRD 3000 T/T) to complete the characterization of the precipitate layer. Calculation of bond distances, bond angles, etc., was carried out using ATOMS V.6.1.2. (2004, Shape Software). Crystal morphologies were simulated using SHAPE V.7.1.2. (2004, Shape Software).

Results and Discussion

Removal of Dissolved As(V) and Release of Calcium as a Function of Time. Figure 1 shows the evolution of the concentration of arsenic, calcium, and sulfate in the aqueous solution during the interaction process. At the very beginning of the experiment, the aqueous solution is obviously free of calcium, but as the gypsum grains dissolve the concentration increases dramatically to reach a maximum during the first ~24 h of reaction. The calcium concentration then decreases slightly toward a limiting value. The sulfate concentration increases simultaneously at a greater rate, reaching a higher asymptotic value. In contrast, the arsenic concentration decreases progressively to approach its asymptotic value after prolonged (~10 days) reaction times. This decrease is accompanied by a small reduction of pH, which progressively approaches a limiting value of about 6.7. Table 1 is displays the analytical concentration (C_0) of the parent solution and the asymptotic concentration (C_∞) of calcium, sulfate, and arsenate. The column $|C_0 - C_\infty|$ represents the number of moles removed from (or released to) one liter of solution after prolonged (20 days) reaction times. The concentration of sodium was determined to be virtually constant (≈180 mmol/L) during the process.

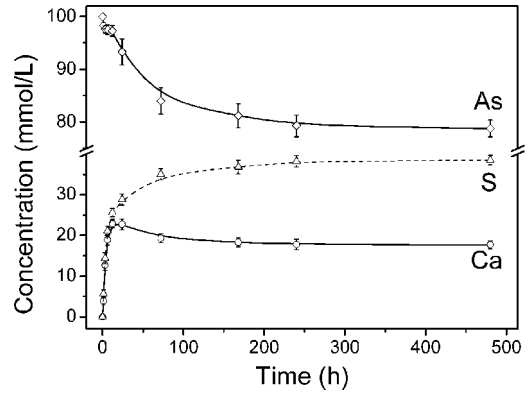

Figure 1. Evolution of As, Ca, and sulfate concentrations as a function of time. The datapoints correspond to the average of five analogous experimental runs. The curves represent a cubic B-spline connection among the average values of these five runs.

Table 1. Initial (C_0) and Final (C_∞) Concentrations of the Reactants in the Aqueous Solution[a]

constituent	C_0 (mmol/L)	C_∞ (mmol/L)	$\lvert C_0 - C_\infty \rvert$(mmol/L)
Ca	0.0	18 ± 1	18
S(VI)	0.0	38 ± 2	38
As(V)	100	79 ± 2	21

[a] The standard deviations are shown with the ± symbol.

It is worth noting that (under the unavoidable analytical error) the difference between the final concentration of sulfate and calcium (38–18 = 20 mmol/L) practically equals the amount of arsenic (≈21 mmol/L) removed from the fluid. This relationship also holds true for intermediate reaction times and obviously points toward a simple coupling between removal and dissolution: as gypsum dissolves, a part of the released calcium reacts with the dissolved arsenate to form a compound containing equimolar quantities of calcium and arsenic. Therefore, taking the prevailing arsenic species in the experimental pH range are $HAsO_4^{2-}$and $H_2AsO_4^-$ into account, the previous observations indicate a coupled dissolution–crystallization process that leads to formation of an acidic calcium arsenate. On the other hand, the asymptotic tendency of all the parameters seems to indicate that the system is virtually at equilibrium at the end of the experiments (20 days). We will study this aspect with the help of the geochemical code PHREEQC in the specific section titled "Reaction Paths and Equilibrium Endpoints".

Overgrowing Crystals: Nature and Morphology. A microscopic observation of the reacting solids confirms that the removal of arsenic occurs by surface precipitation of an acidic calcium arsenate. After an interaction period of less than 12 h, the gypsum grains begin to be covered by a set of micron-sized tabular crystals that grow attached to the fragment contours. As can be observed in Figure 2a, the gypsum surface shows clear dissolution signs, and the newly formed crystals seem to be stuck into the substrate, especially at the tracks marked by the cleavage (010) planes on the contour. Although the overall aspect is a little chaotic, there is a clear nonrandom orientation. After a while, this new phase develops to form an oriented overgrowth onto (010), to finally cover the entire substrate in less than 72 h (Figure 2b).

Although the neoformed crystals exhibit tabular morphologies during the first stages of growth, the most developed crystals have a prismatic shape. The crystals range in length from 20 up to 500 μm, the maximum thickness being about 20–40 μm. The EDS analyses indicate that this phase is composed of calcium, arsenic, and oxygen, yielding atomic ratios of 1 and 6

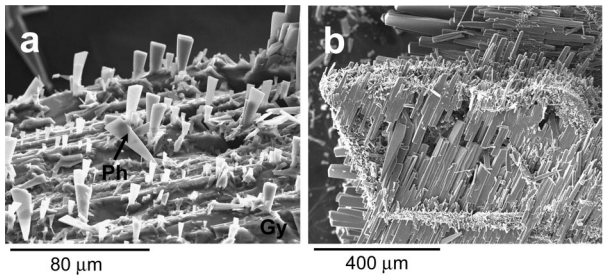

Figure 2. (a) SEM of newly pharmacolite (Ph) crystals at the early stages of the experiment. The crystals are attached to the irregular contour of a gypsum (Gy) cleavage fragment that shows clear signs of dissolution. (b) SEM image of a gypsum grain completely coated by pharmacolite crystals.

for As/Ca and As/O, respectively. Observations using backscattered electrons show no compositional contrast within these solids. Moreover, the presence of S or Na has not been detected. These results are in good agreement with the X-ray diffraction (XRD) data, which indicate the presence of the typical reflections of pharmacolite (at d Å ~7.76, 3.85, 2.71, etc.).

Pharmacolite ($CaHAsO_4 \cdot 2H_2O$) is a calcium arsenate dihydrate with monoprotonated arsenate groups ($HAsO_4^{2-}$) and a monoclinic (*Aa*) structure.[22,23] The structure consists of (020) layers of [AsO_4] tetrahedra alternating with [CaO_8] irregular polyhedra. Two of the oxygen atoms of the calcium polyhedra belong to water molecules, while one of the oxygens of the [AsO_4] group is attached to the acidic hydrogen and is not shared with any other polyhedra. These layers are linked to each other by water molecules via hydrogen bonds, which connect one oxygen of the [AsO_4] tetrahedra with another oxygen of the [CaO_8] octahedra. Hydrogen bonds connect also the [AsO_4] tetrahedra among them, forming chains along [101] within the (020) layers. Although pharmacolite and gypsum are not isostructural, their structures are rather similar, the main differences being the orientation and distortion of the [AsO_4] tetrahedra in pharmacolite as compared with the [SO_4] tetrahedra in gypsum. Moreover, one of the oxygen atoms in the [AsO_4] tetrahedra is attached to a hydrogen atom, thereby forming an acidic arsenate $[HAsO_4]^{2-}$ group. Because of these differences, pharmacolite crystallizes in the polar space group *Aa*, instead of *A2/a*.

The described structural characteristics clearly point to the pinacoid {010} as the potentially dominating form in pharmacolite, which is in agreement with the observed morphologies. Figure 3 illustrates the typical morphology of the crystals formed in the early stages of the experiment. As can be observed, the crystals are formed by {010} plates elongated in the [101] direction. The side faces are poorly developed and are difficult to identify due to their small size and to their nonsingular, curved appearance.

It is worth noting that, in order to facilitate a comparison with the gypsum structure, we have not chosen the setting of the unit cell that appears in the original papers by Ferraris[22,23] but that chosen by Heijnen and Hartman.[24] The crystal structure of gypsum is often described in an *I*-centered space group where the *c*-axis does not correspond to the morphological *c*-axis, which is the direction along which the plates {010} are usually elongated. In an attempt to settle this question, Heijnen and Hartman use the setting of De Jong and Bouman[25] *A2/a*, such that the structural *c*-axis coincides with the morphological one. In the same way, pharmacolite is usually described in an *I*-centered space group. In both settings, the cell parameters *a* (5.975 Å) and *b* (15.434 Å) are analogous but *c* and β differ,

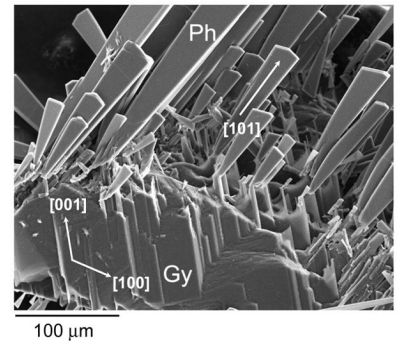

Figure 3. Morphology of pharmacolite (Ph) crystals formed during the early stages of the experiment. The shape is dominated by {010} plates elongated in the [101] direction. The cleavage planes (010) and the directions [100] and [001] of the gypsum (Gy) substrate can also be observed.

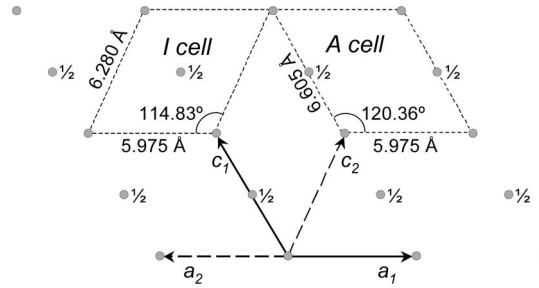

Figure 4. Projection of the pharmacolite lattice on (010) showing the unit cell vectors of the two (*I*-centered and *A*-centered) cell choices.

being 6.605 Å and 120.36°, respectively, in the *Aa* setting used here. Figure 4 shows the projection of the pharmacolite lattice along [010] with the two cell choices outlined by dashed lines. Inspection of this figure shows that the *I*-centered unit cell vectors ($\mathbf{a}_2$, $\mathbf{b}_2$, and $\mathbf{c}_2$) can be written in terms of the *A*-centered cell vectors ($\mathbf{a}_1$, $\mathbf{b}_1$, and $\mathbf{c}_1$) as follows:

$$\mathbf{a}_2 = -\mathbf{a}_1; \mathbf{b}_2 = -\mathbf{b}_1; \mathbf{c}_2 = \mathbf{a}_1 + \mathbf{c}_1 \quad (1)$$

Therefore, the indices of the planes transform with this change of basis according to

$$\begin{bmatrix} h_2 \\ k_2 \\ l_2 \end{bmatrix} = \begin{bmatrix} -1 & 0 & 0 \\ 0 & -1 & 0 \\ 1 & 0 & 1 \end{bmatrix} \begin{bmatrix} h_1 \\ k_1 \\ l_1 \end{bmatrix} = \begin{bmatrix} -h_1 \\ -k_1 \\ h_1 + l_1 \end{bmatrix} \quad (2)$$

Figure 4 also shows that the *c*-axis of the *I*-cell coincides with the [101] direction of the *A*-setting.

As the crystals grow, their shape becomes more prismatic, with {010} as the dominant form, the side forms being $\{\bar{1}11\}$, {111}, {011}, and their corresponding polar counterparts, that is, $\{1\bar{1}\bar{1}\}$, $\{\bar{1}\bar{1}\bar{1}\}$, $\{0\bar{1}\bar{1}\}$. The simulations in Figure 5 show how a combination of these forms can result in the morphologies observed in the present experiments. In those schemes, the dominant (010) face is delimited by <101>, <100>, and $<10\bar{1}>$ edges as a result of the intersection with the side faces. The crystals are elongated on [101], which is the dominating edge in all the crystals observed here. This morphology agrees with the classical morphology reported by Groth,[26] although in the present case the small side form {131} rarely occurs (note that in Groth[26] the choice of axes differs from the one used here).

It is worth noting that, in contrast with the typical gypsum morphologies, the [001] edge does not appear in the pharma-

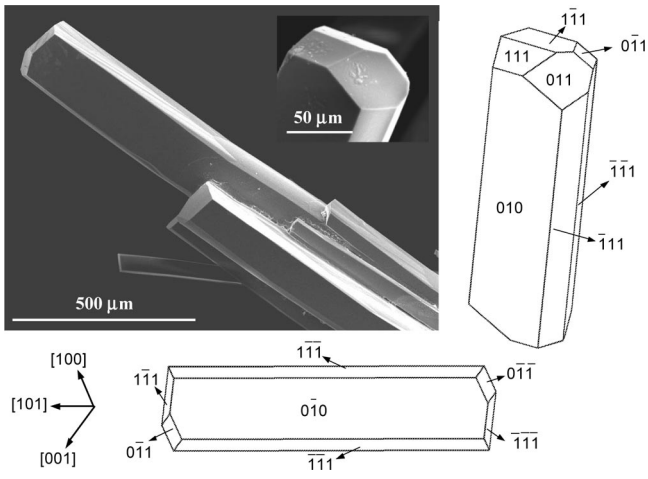

Figure 5. Morphology of pharmacolite crystals. The sketch on the right shows a simulation in which some symmetry-equivalent faces have an unequal development. Towards the lower part, the directions [100], [001], and [101] of the three main PBCs contained within a (020) slice are shown along with the typical pharmacolite habit observed in these experiments.

colite crystals obtained in these experiments. In gypsum the [001] edges usually correspond with the intersection of (010) with (120) or with the intersection between two faces belonging to the {120} form. This last form, however, is unusual in pharmacolite crystals. Moreover, whereas gypsum crystals tend to be elongated on [001], pharmacolite crystals tend to be elongated on [101]. An explanation of these differences requires further consideration of the bond arrangement in both structures, which will be discussed in the next section.

Structure and Morphology of Pharmacolite and Gypsum: A Comparison. Heijnen and Hartman[24] propose six PBCs (Periodical Bond Chains[27]) for the gypsum structure: <100>, <001>, <101>, <0½½>, <1½½>, and <201> arranged in increasing order of period length. These six PBCs give rise to five F forms {020}, {120}, {011}, {$\bar{1}$11}, and {$\bar{1}$22}. Although these authors do not study the pharmacolite bonding arrangement in depth, they assume that for pharmacolite the PBCs are the same and that they lead to the same F forms. In general terms, this assumption is reasonable given the structural similarities between gypsum and pharmacolite. Nevertheless, the difference in the hydrogen bond arrangement and other peculiarities should be considered in order to explain the significant morphological differences observed.

Of the six gypsum PBCs, only <0½½> and <1½½> intersect the (020) slices. These PBCs are not very strong as they involve not only Ca−SO_4 bonds but also hydrogen bonds and Ca−water bonds, according to the sequence Ca−SO−H_2O−Ca. The other four, <100>, <001>, <101>, and <201>, are contained within the (020) slices. The PBC <001> is a direct chain of Ca-SO_4 links in which Ca has short distances to two oxygens of the same SO_4^{2-} group. The PBC <100> is also formed by Ca−SO_4 links but in this case with only one Ca−O short distance. Figure 6a shows the projection of a gypsum (020) slice in which the PBCs along [001], [100], and [101] can be observed. The segments p_1, p_2, and q connect Ca and O atoms within these PBCs. The involved Ca−O distances are displayed in Figure 6b. To a first approximation, one can correlate the distance (R_{ij}) between two atoms with the strength (s_{ij}) of the corresponding bond using the classical bond-valence equation:

$$s_{ij} = \exp[(R_0 - R_{ij})/B] \quad (3)$$

where R_0 and B are fitted constants, R_0 being the length of a bond of unit valence. The bond-valence method is well-documented[28,30] and has been checked with numerous structures. Here the values of R_0 and B for Ca−O bonds (1.967 Å and 0.37, respectively) have been taken from the "bvparm2006.cif" database compiled by Brown.[31] The bond lengths R_{ij} correspond to the experimental Ca−O distances and have been calculated from the atomic positions in the structure. Figure 6b displays these selected bond distances and the corresponding bond strengths as well as a perspective view of the PBCs along [001], [100], and [001]. As can be observed, the repeating period on [001] is longer than that on [100]. However, the PBC along [001] is stronger than that along [100] due to the double Ca−O connections (Ca−O1 and Ca−O2) of the first one. The PBC along [101] is more "out-of-the-way" as it is a zigzag arrangement of alternating "$p_1 + p_2$" and "q" links which form a chain with a longer (6.52 Å) repeating period. Finally, each water molecule is involved in two hydrogen bonds, one of them (O_W−H1−O1) connecting adjacent (020) slices and the other (O_w−H2−O1) laying within the (020) slices to form part of the PBC <201>. This last PBC seems to be the weakest one and is formed by the sequence Ca−H_2O−SO_4−H_2O−Ca.

According to the previous discussion, the PBC <001> is clearly the strongest one. The PBC <100> is second; thus, the slice (020) contains the two most important PBCs in the gypsum structure. Although the PBC method is only an approximation, the perfect (020) cleavage is consistent with this arrangement of PBCs, and the direction [001] of the strongest PBC corresponds with the usual elongation direction (the fiber axis in the satin spar variety of gypsum).

It is worth noting that in the gypsum structure there are only three independent (nonequivalent by symmetry) oxygen positions. Two of them (O_1 and O_2) belong to the SO_4 groups and the other one (O_W) belongs to a water molecule. The sum of all the bond strengths ($V_i = \Sigma s_{ij}$) that each one of these oxygens receives from the adjacent (Ca, S, and H) atoms is reasonably close to the ideal value (2 v.u.) in all cases, which support the suitability of eq 3 to estimate bond strengths in the gypsum structure.

In spite of the structural analogies with gypsum, the bond arrangement in pharmacolite is rather different. The presence of the acidic arsenate group $HAsO_4^{2-}$ not only implies a distortion in the bonding sketch due to the greater size of this ion, but also the anionic hydrogen atoms introduce an important change in the bonding system because they form hydrogen bridges that connect adjacent arsenate tetrahedra. Moreover, the four oxygens in the AsO_4 tetrahedra are crystallographically independent, so that p_1 and p_2 (see Figure 6a) split into four nonequivalent links (p_1, p_2, p_3, and p_4). As a consequence, the PBC along [001] is rather different from its gypsum counterpart. Figure 7a shows a projection of a pharmacolite (020) slice in which this PBC can be observed. As in the gypsum structure, the PBC along [001] is a direct chain of Ca−AsO_4 links, but in this case each Ca has short distances (p_2 = 2.47 Å and p_4 = 2.50 Å) only to one of the oxygens of each adjacent arsenate group. The distance Ca−O_1 is considerably larger (p_1= 2.962 Å) than its equivalent in the gypsum structure. Moreover, this oxygen O_1 is attached to the anionic hydrogen atom at a distance of 1.06 Å. Something similar occurs with the distance Ca−O_3 (p_3 = 2.66 Å). The bond strengths involved in these two interactions are quite low (0.07 v.u. for p_1 and 0.15 v.u. for p_3) so that their contribution to the PBC strength is small as compared to p_2 and p_4. As can be observed in Figure 7b, the repeating period along <001> is larger than that of gypsum.

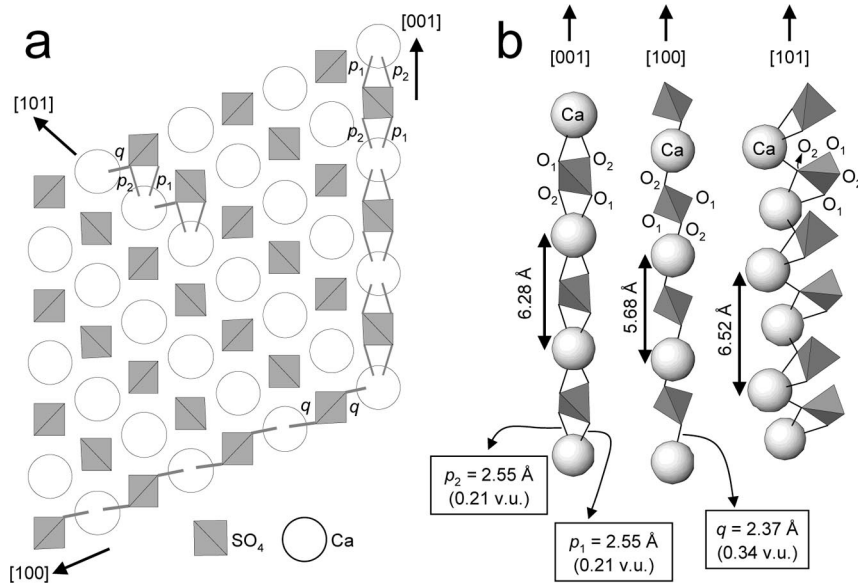

Figure 6. (a) Projection of a (020) slice of the gypsum structure (the water molecules have not been represented). The labels p_1, p_2, and q stand for the Ca−O bonds involved in the PBCs contained within this slice. (b) Perspective view of the PBCs <100>, <001>, and <101>. Repeating periods, bond lengths, and bond strengths (in valence units) are also displayed. Note that the two oxygens O_1 of each SO_4 tetrahedron are in symmetry-equivalent positions. The same holds for the two oxygens labelled O_2.

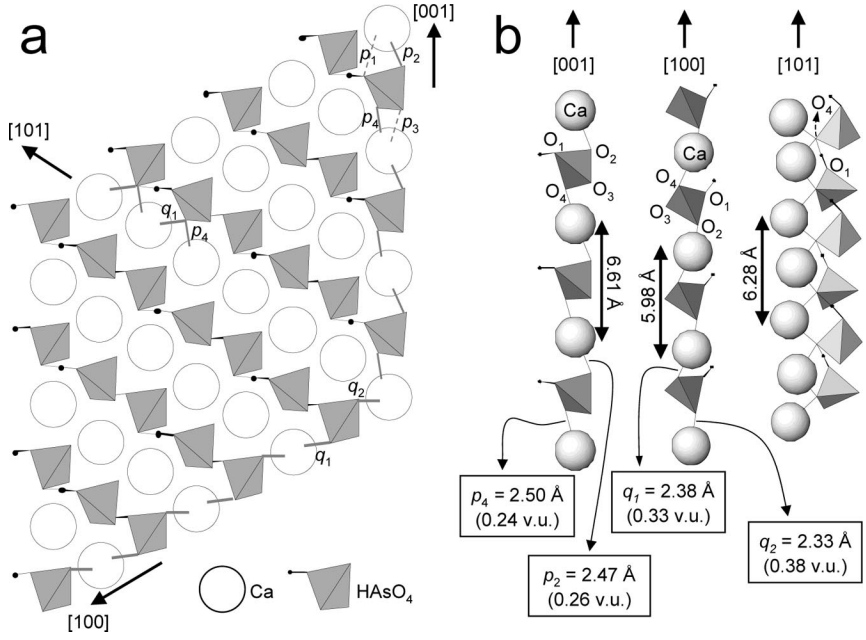

Figure 7. (a) Projection of a (020) slice of the pharmacolite structure (the water molecules have not been represented). The labels p_1, p_2, p_3, p_4, q_1, and q_2 stand for the Ca−O bonds involved in the PBCs contained within this slice. The links p_1 and p_3 (dashed lines) correspond to relatively long distances and have a small influence on the strength of the PBC <001>. (b) Perspective view of the PBCs <100>, <001>, and <101>. Repeating periods, bond lengths, and bond strengths (in valence units) are also displayed. Note the hydrogen bridges along [101].

As a result, this PBC appears to be considerably less important in pharmacolite than in gypsum, in agreement with the morphological differences observed.

The PBC along [100] is quite similar to that of gypsum, although in this case there are two (q_1, and q_2) similar but nonequivalent Ca-O links. In contrast, the PBC along [101] is very different. Whereas there is a similar zigzag arrangement of alternating p and q links between Ca and AsO_4 groups, in pharmacolite this PBC is reinforced by the simultaneous presence of a chain of hydrogen bridges (O_1−H···O_4) connecting adjacent arsenate groups in the [101] direction (see Figure 7). These chains of hydrogen bridges were disregarded by Heijnen and Harmant,[24] but their influence cannot be ignored. As in the phosphate analogue brushite,[32] $CaHPO_4 \cdot 2H_2O$, the involved hydrogen bridge is the strongest one in the pharmacolite structure, with a short distance of 1.67 Å to O_4 and an angle O_1−H···O_4 of 166.7°. Although calculations of hydrogen bonds with empirical models are not straightforward, a simple estimation of the strength of this bond using Brown's database[31] ($R_0 = 0.569$ Å and $B = 0.94$ for 1.05 Å < O−H <1.7 Å) gives a value of 0.31 v.u. The water hydrogen atoms form bridges with

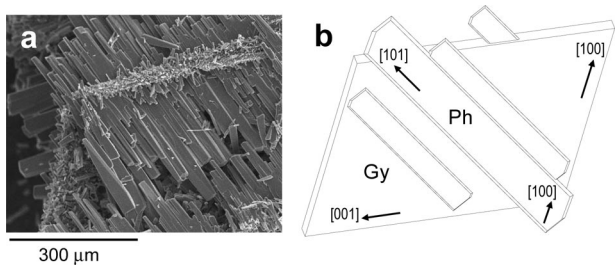

Figure 8. (a) SEM image of pharmacolite crystals grown onto the (010) surface of a gypsum grain. The original contour of the gypsum grain is marked by a precipitate of smaller crystallites. (b) Epitaxial relationships between gypsum (Gy) and pharmacolite (Ph) crystals. An *A*-centered unit-cell setting has been used for both minerals.

the other three oxygens O_1, O_2, O_3 of the tetrahedra, but the corresponding strengths were estimated to be lower (≈0.25 v.u.).

The previous observations explain the morphological predominance of [101] in pharmacolite as well as the low significance of [001]. In fact, the strong bonding along [101] becomes evident after a simple comparison between the unit-cell shapes of pharmacolite and gypsum. Whereas the repeating periods along [001] and [100] are larger in pharmacolite than in gypsum, the repeating period along [101] is considerably shorter (6.28 Å in pharmacolite against 6.52 Å in gypsum). The unit cell of pharmacolite is accordingly contracted along [101] and the β angle result is significantly larger (120.4° in pharmacolite against 114.1° in gypsum).

Epitaxial Relationships between Pharmacolite and Gypsum. One of the most significant features of the interaction process is that pharmacolite crystallization occurs in a nonrandom orientation. The pharmacolite crystals grow with their elongation direction following the [101] direction of the gypsum substrate. Although we are dealing with a sort of solvent-mediated replacement of gypsum for pharmacolite, this "oriented overgrowth" can be interpreted as an "epitaxy" as the guest crystals grow subsequently on the surface of the host crystals.[33] A detailed view of this overgrowth is shown in Figure 8, which also shows a simulation of the epitaxial relationships. Using an *A*-centered unit-cell setting for both minerals, the epitaxy can be characterized by considering the matching between the two structures along the common [101] direction. When the thickness of the overgrowth is comparable to the thickness of the substrate, the mismatch (f) is usually described by the expression:[34]

$$f = \frac{2(p_s - p_o)}{p_s + p_o} \tag{4}$$

where p is the repeating period along the matching directions of substrate (s) and overgrowth (o). For pharmacolite and gypsum, the repeating periods along [101] are 6.28 and 6.52 Å, respectively. This means a misfit with an absolute value of about 3.8%, which is clearly within the limits required for epitaxial nucleation from solution.[35] Given that $p_s < p_o$, the sign of this misfit is negative. The simultaneous matching along other equivalent directions on (010) is, however, more problematic. If one compares the repeating periods of pharmacolite and gypsum along [100] and [001], one obtains misfits of about 5.0 and 5.1%, respectively. These misfits are still moderate but, in contrast with the misfit along [101], their signs are positive since $p_s > p_o$ along both directions. As previously shown, the unit cell of pharmacolite is relatively "contracted" along [101], and the resulting β angle is significantly larger for pharmacolite (120.4°) than for gypsum (114.1°); that is, there is an angular misfit of about 6.3°. For that reason, the pharmacolite overgrowth does not form continuous layers or thin platelets on the surface, but thick three-dimensional crystals elongated on [101]. These observations point toward a Volmer–Weber mechanism,[36] which is characteristic of weak adhesion between substrate and overgrowth. Moreover, the arrangement of the crystals formed in the early stages of the experiment (see Figure 3) suggests that the reticular control could be essentially one-dimensional, with [101] as the correspondence direction.

In reality, the morphological features of pharmacolite support the *I*-centered unit-cell as the best choice to describe its structure. Changing (eq 2) from *Aa* to an *Ia* setting, the elongation direction [101] becomes [001]; that is, the structural c axis becomes coincident with the direction of maximum morphological importance in pharmacolite. Finally, keeping the *A2/a* space group[25] for gypsum and using the original[22] *Ia* for pharmacolite, the epitaxial relationship becomes $(010)_{Gy} \parallel (010)_{Ph}$ and $[101]_{Gy} \parallel [001]_{Ph}$.

Reaction Paths and Equilibrium End Points. This work shows that, around a pH of 7, the interaction of dissolved As(V) and gypsum results in surface precipitation of pharmacolite crystals. Such a process involves the release of solutes (Ca^{2+} and SO_4^{2-} ions) from the gypsum surface to the fluid and the reaction between the released Ca^{2+} and the aqueous $HAsO_4^{2-}$ ions to form pharmacolite nuclei. Thus, gypsum dissolution is concomitant with surface precipitation, and the reaction could be envisaged as a sort of solvent-mediated replacement of gypsum by pharmacolite according to

$$HAsO_{4\,(aq)}^{2-} + CaSO_4 \cdot 2H_2O_{(s)} \leftrightarrow CaHAsO_4 \cdot 2H_2O_{(s)} + SO_{4\,(aq)}^{2-} \tag{5}$$

where the subscripts aq and s stand for aqueous species and solid phases, respectively. To determine the driving forces operating during the experiments, the activities of the aqueous species (free ions and complexes) have been calculated by applying PHREEQC to the experimental data (solution pH and analytical concentrations of As, Ca, Na, and sulfate). With this aim, the PHREEQC database was completed for the aqueous species AsO_4^{3-}, $HAsO_4^{2-}$, $H_2AsO_4^{-}$, $H_3AsO_4^{0}$, $CaAsO_4^{-}$, $CaHAsO_4^{0}$, and $CaH_2AsO_4^{+}$ using the stability constants compiled by Bothe and Brown.[19] In the output, PHREEQC displays concentrations and activities of all the aqueous species and the saturation index with respect to all the relevant solid phases. The saturation index (SI) is a measure of the supersaturation and is given by:

$$SI = \log \frac{\Pi a_i^{v_i}}{K_{sp}} \tag{6}$$

where $\Pi a_i^{v_i}$ stands for the product of ion activities in the aqueous solution, v_i is the stoichiometric number of the ion i in the solid formula, and K_{sp} stands for the thermodynamic solubility product of the solid phase. Obviously, SI = 0 reflects equilibrium, SI < 0 subsaturation, and SI > 0 supersaturation. Unfortunately, to the authors' knowledge, the thermodynamic solubility product of pharmacolite and many other calcium arsenates is unknown. This occurs because many calcium arsenates are difficult to produce as phase-pure, but they are most readily formed in conjunction with other phases[19] (a mixture of different hydrates, different protonation degrees, etc.). Here the solubility product of pharmacolite has been estimated assuming that the aqueous solution is at equilibrium with pharmacolite at the end of the experiments (480 h), which seems to be reasonable if one

Table 2. Activities (a_i) of the Aqueous Ca^{2+}, $HAsO_4^{2-}$, and SO_4^{2-} Ions as a Function of Time[a]

time (h)	$a(HAsO_4^{2-}) \times 10^3$	$a(Ca^{2+}) \times 10^3$	$a(SO_4^{2-}) \times 10^3$
0	24.0	0.00	0.0
1	22.6 ± 0.2	0.28 ± 0.08	1.2 ± 0.2
3	20.3 ± 0.2	1.0 ± 0.1	3.0 ± 0.3
6	19.2 ± 0.1	1.5 ± 0.1	4.2 ± 0.2
12	18.4 ± 0.1	1.82 ± 0.06	5.0 ± 0.2
24	17.4 ± 0.3	1.83 ± 0.09	5.7 ± 0.3
72	15.5 ± 0.4	1.64 ± 0.08	7.0 ± 0.4
168	14.4 ± 0.3	1.58 ± 0.08	7.4 ± 0.3
240	13.8 ± 0.3	1.57 ± 0.09	7.7 ± 0.3
480	13.7 ± 0.2	1.55 ± 0.07	7.8 ± 0.2

[a] Mean of the values calculated for each of the five replicate analytical data. The standard deviations are shown with the ± symbol.

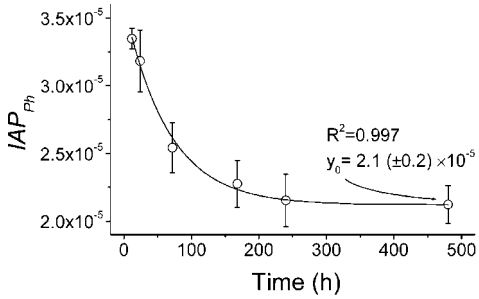

Figure 9. Evolution of IAP_{Ph} between 12 and 480 h of reaction. The data points have been fitted to an exponential decay function. The asymptotic limit (y_0) and the coefficient of determination (R^2) are also shown.

considers the asymptotic shape of the analytical data (see Figure 1). The composition of the aqueous solution remains virtually unchanged (<2%) during the last 10 days of the experiment. Moreover, the final concentration is virtually the same in the five replicate experiments, the relative standard deviation being less than 2%. This asymptotic tendency can also be observed in Table 2, which displays the activities (calculated with PHREEQC) of the relevant aqueous species (Ca^{2+}, $HAsO_4^{2-}$, and SO_4^{2-}) as a function of time.

From the activities of Ca^{2+} and $HAsO_4^{2-}$, the ionic activity product (IAP) corresponding to pharmacolite can be calculated, according to the following expression:

$$IAP_{Ph} = \sum \Pi a_i^{\nu_i} = a(HAsO_4^{2-}) \cdot a(Ca^{2+}) \qquad (7)$$

The evolution of this activity product is shown in Figure 9, which represents the decrease of IAP_{Ph} between 12 and 480 h of reaction. The data points have been fitted to an exponential decay function, the asymptotic limit being $y_0 = 2.1 \times 10^{-5}$. This limit can be considered as a reasonable estimation of the thermodynamic solubility product, since at equilibrium IAP = K_{sp}. The result corresponds to a pK ($-\log K_{sp}$) of 4.68 ± 0.04 and is close to the solubility product estimated for haidingerite (pK = 4.74),[19] another acidic calcium arsenate hydrate ($CaHAsO_4 \cdot H_2O$). The newly obtained solubility product of pharmacolite can now be used in PHREEQC to calculate the evolution of the saturation index with respect to this phase.

Figure 10 shows the evolution of the saturation index of the experimental solution with respect to pharmacolite and gypsum. At the very beginning of the experiment, the aqueous solution is obviously undersaturated with respect to both phases, but the fast dissolution of the gypsum grains leads to a dramatic increase of the saturation indices. The fluid quickly becomes supersaturated with respect to pharmacolite, reaching a maximum ($SI_{Ph} \approx 0.2$) during the first 12 h of the experiment. Afterward, the uninterrupted growth of pharmacolite leads to a decrease of As(V) concentration

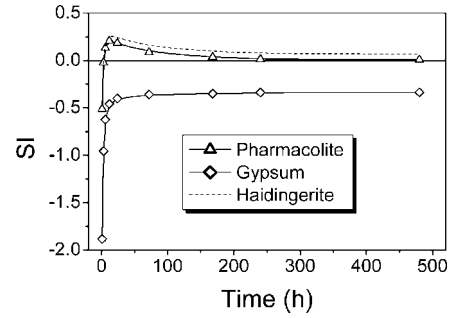

Figure 10. Evolution of the saturation index of the experimental solution with respect to pharmacolite and gypsum as a function of time. Although formation of haidingerite has not been detected, the evolution of the saturation index with respect to this phase is also shown (see discussion in text). The curves represent a cubic B-spline connection among the average values of the five replicate experiments. The horizontal line at SI = 0 corresponds to equilibrium.

in the fluid, and SI_{Ph} gradually approaches zero. The saturation index with respect to gypsum evolves differently, and although it increases quickly in the first hours, the aqueous solution remains undersaturated with respect to this phase during the whole experiment. Everything seems to indicate that equilibrium with respect to gypsum, the dissolving phase, will be never reached as the SI curve tends to an asymptotic value around −0.34.

The previous scenario could be explained as a result of the covering of the gypsum surface. During the process, the surface precipitate can protect the substrate from further dissolution, so that the process stops, at least on a laboratory time scale. In fact, the development of a crust of pharmacolite that completely covers the gypsum grains have been observed in all the SEM images taken at the end of the experiment (see Figure 2b). Obviously, at this stage the system is not at equilibrium, but the term[37] "partial equilibrium" could be used to describe a situation in which the reactive solid becomes isolated from the aqueous solution by a coating of secondary solids.

Figure 10 also displays the saturation index (dashed line) corresponding to haidingerite. This mineral only differs from pharmacolite in the number of water molecules, so that its ionic activity product is also given by eq 7. As a consequence, the haidingerite curve parallels the pharmacolite curve, the supersaturation for haindigerite being always higher due to its lower solubility. In spite of this, neither XRD nor SEM−EDS have detected formation of haindigerite at any stage of the process. The situation is anomalous in some way since haidingerite is less soluble and would be more likely to nucleate. There are two possible explanations for this behavior. First of all, it could be a result of a lack of precision in the estimation of the solubility. Pharmacolite solubility seems to very similar to that of haidingerite, and a small error in the determination of one of these two solubility products could be enough to change their relative value. The determination solubility products for calcium arsenates presents important difficulties, and it is frequently carried out by precipitation experiments in which an assemblage of two or more solid phases is formed.[19] In such experiments, equilibrium is assumed to occur when, after a while, no change in the aqueous solution composition is observed and the solid phase assemblage remains unaltered. This assumption is, however, questionable as reaching a true equilibrium situation (at an invariant point) could require a dissolution−recrystallization process involving extremely slow changes, which is difficult to detect. In this context, the present experiments have the advantage that, while gypsum and pharmacolite coexist in the system, the gypsum grains are completely coated by pharmacolite crystals and, in practice, equilibrium only involves pharmacolite.

A second possibility is related to the epitaxial relationships between pharmacolite and gypsum. The metastable, heterogeneous nucleation of pharmacolite on gypsum could be favored by the structural similarities between both phases. In fact, the supersaturation level during the whole process is not very high, and the reduction of the nucleation barrier due to the structural matching gypsum-pharmacolite could be decisive. Equilibrium with respect to haidingerite is not reached after rather prolonged times (480 h), but the final saturation index is very low (<0.1) and could be insufficient to nucleate haidingerite.

As a final point, it is interesting to consider the maximum As(V) concentration that can exist in the presence of gypsum within this pH range. As previously discussed, the asymptotic limit does not represent a "true equilibrium" end point but a "partial equilibrium" situation[37] in which the reactive solid becomes isolated from the aqueous solution by a coating of secondary solids. The true equilibrium end point would imply simultaneous equilibrium of both pharmacolite and gypsum with the aqueous solution, according to eq 5. The equilibrium constant for this reaction can be easily derived from the solubility products of pharmacolite and gypsum:

$$K = \frac{a(SO_4^{2-})}{a(HAsO_4^{2-})} = \frac{a(Ca^{2+}) \cdot a(SO_4^{2-})}{a(Ca^{2+}) \cdot a(HAsO_4^{2-})} = \frac{K_{sp}(Gy)}{K_{sp}(Ph)} = \frac{10^{-4.58}}{10^{-4.68}} = 10^{0.1} \quad (8)$$

This means that, at equilibrium, the ratio between the activities of SO_4^{2-} and $HAsO_4^{2-}$ in the aqueous solution has to be constant and equal to $10^{0.1} \approx 1.26$. However, the actual ratio at the end of the experiments was ≈0.57 (see Table 2), which clearly indicates that equilibrium has not been reached and that there is an excess of arsenate in the aqueous solution. For the composition and pH of the aqueous solution used in these experiments, the true equilibrium end point can be calculated using the tool "equilibrium phases" in PHREEQC. The program gives a total As(V) concentration of around 61 mmol/L as output, the activity of $HAsO_4^{2-}$ being 9.6×10^{-3}. To reach this situation the surface covering should be incomplete, which would require the presence of a sufficient amount of gypsum solids.

Conclusions

At neutral pH the interaction of arsenate-bearing aqueous solutions with gypsum results in surface precipitation of pharmacolite crystals. Because of the structural similarities between both phases, the crystals grow oriented onto the gypsum surface, forming an epitaxy. The solubility of pharmacolite has been determined to be fairly high ($pK = 4.68 \pm 0.04$), and the limiting As(V) concentration in the aqueous solution at the "true equilibrium" end point has been computed to be around 61 mmol/L. This concentration represents the minimum arsenate level that can be attained, at neutral pH, using gypsum. As expected, this amount is extremely high from the perspective of water quality, and thus gypsum does not seem to be a suitable remediation tool in this pH range. What is more, due to the epitaxial coating the process can stop prematurely at a "partial equilibrium endpoint", when only a small fraction of As(V) has been removed from the fluid.

Acknowledgment. This work was supported by the Ministry of Education and Science of Spain (Grant CGL2004-02501). We thank anonymous reviewers and Associate Editor Roger Davey for their insightful comments.

References

(1) Tesoriero, A. J.; Pankow, J. F. *Geochim. Cosmochim. Acta* **1996**, *60*, 1053–1063.
(2) Reeder, R. J. *Geochim. Cosmochim. Acta* **1996**, *60*, 1543–1552.
(3) Godelitsas, A.; Astilleros, J. M.; Hallam, K.; Harissopoulos, S.; Putnis, A. *Environ. Sci. Technol.* **2003**, *37*, 3351–3360.
(4) Köhler, S. J.; Cubillas, P.; Rodríguez-Blanco, J. D.; Bauer, C.; Prieto, M. *Environ. Sci. Technol.* **2007**, *41*, 112–118.
(5) Sposito, G. A. In *Geochemical Processes and Mineral Surfaces*; Davis, J. A., Hayes, K. F., Eds.;*ACS Symposium Series* 1986; Vol. *223*, pp 217–228.
(6) Prieto, M.; Cubillas, P.; Fernández-González, A. *Geochim. Cosmochim. Acta* **2003**, *67*, 3859–3869.
(7) Prieto, M.; Fernández-González, A.; Martín-Díaz, R. *Geochim. Cosmochim. Acta* **2002**, *66*, 783–795.
(8) Andara, A. J.; Heasman, D. M.; Fernández-González, A.; Prieto, M. *Cryst. Growth Des.* **2005**, *5*, 1371–1378.
(9) Fernández-González, A.; Andara, A.; Alía, J. M.; Prieto, M. *Chem. Geol.* **2006**, *225*, 256–265.
(10) Roman-Ross, G.; Charlet, L.; Cuello, G. J.; Tisserand, D. *J. Phys. IV* **2003**, *107*, 1153–1156.
(11) Fernández-Martínez, A.; Román-Ross, G.; Cuello, G. J.; Turrillas, X.; Charlet, L.; Jonson, M. R.; Bardelli, F. *Physica B* **2006**, *385–386*, 935–937.
(12) Juillot, F.; Ildefonse, P.; Morin, G.; Calas, G.; Kersabiec, A. M.; Benedetti, M. *Appl. Geochem.* **1999**, *14*, 1031–1048.
(13) Rodríguez-Blanco, J. D. Interaction of As(V) with gypsum at different pH ranges. Ph.D. Thesis, Universidad de Oviedo, Oviedo, 2006.
(14) Vaughan, D. J. *Elements* **2006**, *2*, 71–75.
(15) Jiménez, A.; Prieto, M.; Salvadó, M. A.; Gracía-Granda, S. *Am. Mineral.* **2004**, *89*, 601–609.
(16) Bothe, J. V.; Brown, P. W. *Environ. Sci. Technol.* **1999**, *33*, 3806–3811.
(17) Twidwell, L. G.; McCloskey, J.; Miranda, P.; Gale, M. In *Rewas'99, Global Symposium on Recycling, Waste Treatment and Clean Technology*; Gaballah, I., Hager, J. P., Solozabal, R., Eds.; The Minerals, Metals and Materials Society: Warrendale, 1999; pp 1715–1726.
(18) Nishimura, T.; Robins, R. G.; Twidwell, L. G. In *Waste Treatment and Environmental Impact in the Mining Industry*; Sánchez, M. A., Vergara, F., Castro, S. H., Eds.;Proceedings of the 5th International Conference on Clean Technologies for the Mining Industry, Santiago de Chile, 2000; Vol. 1, pp 131–141.
(19) Bothe, J. V.; Brown, P. W. *J. Hazard. Mater.* **1999**, *69*, 197–207.
(20) Magalhães, M. C. F. *Pure Appl. Chem.* **2002**, *74*, 1843–1850.
(21) Parkhurst, D. L.; Appelo, C. A. J. *User's Guide to PHREEQC (Version 2) - A Computer Program for Speciation, Batch-Reaction, One-dimensional Transport and Inverse Geochemical Calculations*;U.S. Geological Survey Water Resources Investigations Report 99–4259; U.S. Geological Survey: Washington, DC, 1999.
(22) Ferraris, G. *Acta Crystallogr.* **1969**, *B25*, 1544–1550.
(23) Ferraris, G.; Jones, D. W.; Yerkess, J. *Acta Crystallogr.* **1971**, *B27*, 349–354.
(24) Heijnen, W. M. M.; Hartman, P. *J. Cryst. Growth* **1991**, *108*, 290–300.
(25) De Jong, W. F.; Bouman, J. *Z. Kristallogr.* **1938**, *100*, 275.
(26) Groth, P. *Chemische Krystallographie*; Engelmann: Leipzig, 1908; Vol *II*, p 603.
(27) Woensdregt, C. F. *Faraday Discuss.* **1993**, *95*, 97–107.
(28) Brown, I. D.; Altermatt, D. *Acta Crystallogr.* **1985**, *B41*, 224–247.
(29) Urusov, V. S. *Acta Crystallogr.* **1995**, *B51*, 641–649.
(30) Brown, I. D. *The Chemical Bond in Inorganic Chemistry: The Bond Valence Model*; Oxford University Press: Oxford, 2002; p 279.
(31) Brown, I. D. Accumulated table of bond-valence parameters (bvparm2006.cif); downloaded from http://www.ccp14.ac.uk/ccp/web-mirrors/i_d_brown/bond_valence_param/, 2006.
(32) Sainz-Díaz, C. I.; Villacampa, A.; Otalora, F. *Am. Mineral.* **2004**, *89*, 307–313.
(33) Bonev, I. *Acta Crystallogr.* **1972**, *A28*, 508–512.
(34) Sangwal, K. *Elementary Crystal Growth*; Saan Publishers: Lublin, 1994; p 556.
(35) Walton, A. G. In *Nucleation*; Zettlemoyer, A. C., Ed.; Dekker: New York, 1969; pp 225–307.
(36) Chernov, A. A. *Modern Crystallography III. Crystal Growth*; Springer-Verlag: Berlin, 1984.
(37) Helgeson, H. C. *Geochim. Cosmochim. Acta* **1968**, *55*, 853–877.

CG070222+